Available online at www.sciencedirect.com
SCIENCE DIRECT
Solid State Communications 138 (2006) 353–358
solid state communications
www.elsevier.com/locate/ssc

Phenomenological band structure model of magnetic coupling in semiconductors

Gustavo M. Dalpian [a,1], Su-Huai Wei [a,*], X.G. Gong [b,c], Antônio J.R. da Silva [d], A. Fazzio [d]

[a] National Renewable Energy Laboratory, Basic Science Center, 1617 Cole Blvd., Golden, CO 80401, USA
[b] Department of Physics, Fudan University, Shanghai 200433, China
[c] Institute of Solid State Physics, Chinese Academy of Sciences, Hefei 230031, China
[d] Instituto de Física, Universidade de São Paulo, CP 66318, 05315-970 São Paulo, SP, Brazil

Received 4 January 2006; received in revised form 27 February 2006; accepted 2 March 2006 by H. Ohno
Available online 23 March 2006

Abstract

A unified band structure model is proposed to explain the magnetic ordering in Mn-doped semiconductors. This model is based on the p–d and d–d level repulsions between the Mn ions and host elements and can successfully explain magnetic ordering observed in all Mn doped II–VI and III–V semiconductors such as CdTe, GaAs, ZnO, and GaN. The model can also be used to explain the interesting behavior of GaMnN, which changes from ferromagnetic ordering to antiferromagnetic ordering as the Mn concentration increases. This model, therefore, is useful to provide a simple guideline for future band structure engineering of magnetic semiconductors.

PACS: 75.50.Pp; 71.55.−i; 71.70.−d

Keywords: A. Semiconductor; D. Band structure; D. Magnetic properties

1. Introduction

Transition metal doped II–VI and III–V diluted magnetic semiconductors (DMS) have many unique magneto-optical, magneto-electrical, and magneto-transport properties that are essential for future-generation spintronic device applications [1–5]. These materials also present many interesting behaviors. For example, Mn-doped II–VI semiconductors generally have antiferromagnetic (AFM) ground state, whereas Mn doped III–V semiconductors mostly have ferromagnetic (FM) ground state. More intriguing, some of the systems, such as Mn-doped GaN, can be either FM [6–9] or AFM [10], depending on the material properties and growth conditions. However, the exact nature of the magnetism observed in this system is still under debate [11,12,14]. It is, therefore, quite interesting to understand the mechanisms of magnetic coupling that control the magnetic state in these systems.

The mechanism that is responsible for the magnetic coupling in Mn doped III–V semiconductors has been widely discussed over the last few years [15–18]. Several models have been proposed to explain the phenomena, including the phenomenological Zener/RKKY, superexchange and double exchange models. Although these models are quite successful in explaining magnetic order in some of the systems, they often lack universality and transparency, and are difficult to compare directly with ab initio band structure calculations. In this paper, using a band structure approach and level repulsion model, we will describe a unified picture to explain what controls the magnetic ordering in Mn-doped III–V and II–VI semiconductors and relate the different mechanisms to the previous models. We show through ab initio calculations that our model can successfully explain magnetic ordering observed in all Mn-doped II–VI and III–V semiconductors such as CdTe, GaAs, ZnO, and GaN. It can also explain the intriguing behavior of GaMnN, that was found to be either FM or AFM [6–10,12]. Therefore, our model can provide simple guidelines for future band structure engineering of magnetic semiconductors.

2. Band coupling model

Our model is derived from the coupling and level repulsion between the magnetic ions d and the host p states. When Mn

* Corresponding author. Tel.: +1 303 384 6666; fax: +1 303 384 6432.
E-mail address: swei@nrel.gov (S.-H. Wei).
[1] Present address: University of Texas at Austin, Austin, TX 78712, USA.

0038-1098/$ - see front matter © 2006 Elsevier Ltd. All rights reserved.
doi:10.1016/j.ssc.2006.03.002

atoms are incorporated into a semiconductor, they will introduce d levels either inside [3] the valence band or above [13] the valence band maximum (VBM) of the semiconductor, depending on the host material. For example, for Mn in GaAs and CdTe, the occupied majority d orbitals are below the host VBM, which contains mostly anion p states. The unoccupied minority d orbital is above the VBM. On the other hand, in ZnO and GaN, the d levels are above the VBM. In a tetrahedral crystal field, the Mn d states split into t_{2d} and e_d states, whereas the host p states have the t_{2p} symmetry. The states with the same t_2 symmetry can couple strongly with each other, forming hybrid pd orbitals. Furthermore, without spin–orbit (SO) coupling, only the states with the same spin configuration can couple to each other [19,20]. Fig. 1 shows the possible scenarios for the states that may couple to each other. In Fig. 1(a), the host t_{2p} state is above the magnetic ion t_{2d} state, and the coupling leads to a level repulsion that pushes up the t_{2p} state by Δ^1_{pd} and pushes down the t_{2d} state by Δ^1_{pd}. In Fig. 1(b), the t_{2d} state is above the t_{2p} state, and they are pushed up and down respectively by Δ^2_{pd}. Fig. 1(c) shows the couplings between the two majority spin d levels and the two minority spin d levels, which lead to splittings $2\Delta^1_{dd}$ and $2\Delta^2_{dd}$, respectively. Fig. 1(d) shows the coupling between the majority spin d state and the minority spin d state, which pushes up the minority t_{2d} state by $\Delta^{1,2}_{dd}$ and pushes down the majority spin state by the same amount. The coupling between the e_d states is similar to that of between the t_{2d} states, and they are described in Fig. 1(e) and (f). In principle, the strength of the interactions in Fig. 1 depends on the distance and orientation of the Mn pair. From these figures, we can see that there will be no energy gain if the two coupled states are fully occupied or fully empty. A magnetic state can be stabilized only if there

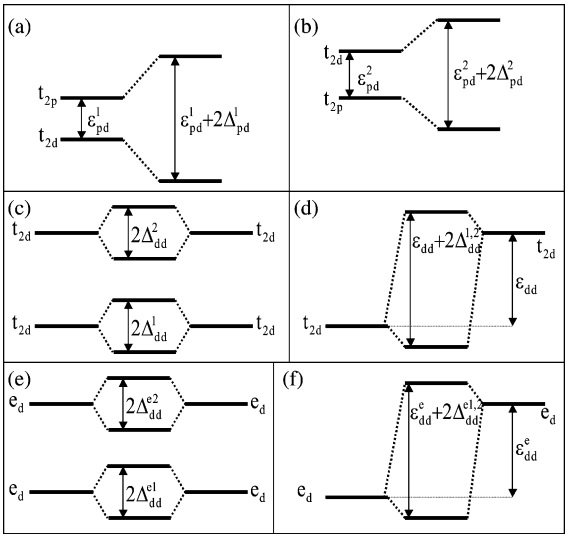

Fig. 1. Schematic model for p–d and d–d couplings. (a) p–d coupling with t_{2p} above t_{2d}. (b) p–d coupling with t_{2p} below t_{2d}. (c) d–d coupling between the t_{2d} states with majority spin level coupled to majority spin level and minority spin level coupled to minority spin level, and (d) d–d coupling between the t_{2d} states with majority spin level coupled to minority spin level. (e) Same as (c), but between the e_d state. (f) Same as (d), but between the e_d state.

are both holes and electrons in the coupled states. Because of the above observation, in the following discussion, we will discuss only the pd coupling between the Mn t_{2d} state and the effective t_{2p} levels at the top of the valence bands, which have large anion p-character. This kind of effective two band coupling model have been widely used in the past to describe p–d coupling in magnetic and non-magnetic semiconductors [18,21]. It has also been used to describe coupling between localized isovalent defect level and host states in dilute isovalent semiconductor alloys (e.g. GaAsN) [22].

In general, the p–d coupling is larger than the d–d coupling because the host p orbital is more delocalized and Mn d and anion p are nearest neighbors. Within the d–d coupling, the coupling between the e_d state is much weaker than the coupling between the t_{2d} state, because the e_d state is very localized, whereas the t_{2d} state is less localized due to the hybridization with the host p states. Because the d–d coupling between the e_d state is qualitatively similar to that of between the t_{2d} state, they are not discussed explicitly in our model. Furthermore, $\Delta^{1,2}_{dd}$ is smaller than Δ^1_{dd} when the exchange splitting ε_{dd} is not zero because the level repulsion is larger if the energy separation of the two coupling states is small.

With the understanding above, in the following, we will discuss the mechanism of magnetic ordering observed in Mn doped II–VI and III–V semiconductors. In the discussion, we will use the effective two-level coupling model described in Fig. 1. First we will discuss the interaction between the p and d levels, and then the interaction between the d levels. We will assume the coupling is additive. The small effect of coupled p–d and d–d interactions will be discussed briefly for simplicity, but in general, the treatment would not change the results qualitatively.

We discuss first the scenario when the VBM is between the Mn majority and minority spin d states. This is the case for most Mn-substituted II–VI and III–V systems such as CdMnTe and GaMnAs. A schematic plot is shown in Fig. 2, where the level repulsions are arranged in spin-up and spin-down channels in FM and AFM configurations. Here, the effective t_{2p} states are the one surrounding the Mn atom with energy at the top of the valence bands. Although the t_{2d} state also couples to other t_{2p} states, these interactions will not result in an energy

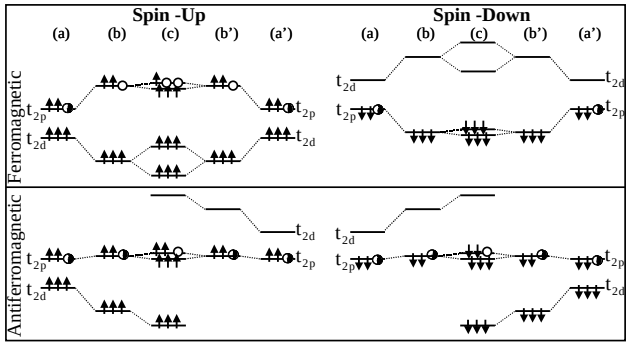

Fig. 2. Schematic model showing the position of the p and d levels and level repulsion between them in FM and AFM configurations. In this case, the VBM is in between the majority and minority d levels. Note that in (b), (b′), and (c), the states have mixed pd characters.

gain if these levels are fully occupied. From (a) to (b) or (a′) to (b′), only the p–d coupling is turned on. From (b) and (b′) to (c), the d–d coupling is turned on. We first look at the FM configuration. In the spin-up channel, the p–d coupling pushes the t_{2p} state upward by $2\Delta^1_{pd}$, whereas it pushes down the t_{2d} state by the same amount. The net energy gain in this process is $-2m_h\Delta^1_{pd}$, where m_h is the number of holes. The d–d coupling further splits the d levels by $2\Delta^1_{dd}$. Because all the t_{2d} majority spin levels are fully occupied, there is no energy gain in this process (the p–p coupling is already included in the band structure calculation for the host, and its effect is the same for FM and AFM cases; therefore, it is not discussed here). In the spin-down channel, the p–d coupling lowers the energy of the occupied t_{2p} spin-down state by $2\Delta^2_{pd}$. Because there are six electrons in the two t_{2p} states, the net energy gain in this case is $-12\Delta^2_{pd}$. Therefore, the net energy gain for the FM configuration is $-2m_h\Delta^1_{pd}-12\Delta^2_{pd}$. In the AFM configuration, the situation is the same in the spin-up and spin-down channel. When the p–d coupling is turned on, the t_{2p} state is pushed up by the occupied majority t_{2d} state by Δ^1_{pd}, but pushed down by the unoccupied minority t_{2d} state by Δ^2_{pd}. The occupied majority t_{2d} state is pushed down by Δ^1_{pd}, and it is further pushed down by the unoccupied minority t_{2d} state by $\Delta^{1,2}_{dd}$. Therefore, the net energy gain in the AFM configuration is $-m_h\Delta^1_{pd}-(12-m_h)\Delta^2_{pd}-6\Delta^{1,2}_{dd}$. Here, in the first-order approximation we assumed that the t_{2p} states are delocalized so it couples with both Mn atoms. In higher-order perturbation theory, the t_{2p} state (and the hole) [23] can be more localized around the Mn atom, so when the Mn atoms are separated by a large distance, the coupling between the Mn atom and the t_{2p} state localized around the other Mn atom is reduced. Taking this consideration into account the energy difference between the FM and AFM phase is

$$\Delta E_{FM-AFM} = -\alpha m_h\left(\Delta^1_{pd}+\Delta^2_{pd}\right)+6\Delta^{1,2}_{dd}, \quad (1)$$

where $\alpha<1$ decreases when the hole states become more localized, and when Mn–Mn distance increases. This result suggests that (a) the AFM phase is stabilized by the energy $6\Delta^{1,2}_{dd}$ from coupling between the majority and minority spin d states (often denoted as superexchange) [24]. (b) The FM phase is stabilized with energy $-\alpha m_h(\Delta^1_{pd}+\Delta^2_{pd})$, which is proportional to the number of holes and the p–d exchange splitting $(\Delta^1_{pd}+\Delta^2_{pd})$, as described in the Zener model. Therefore, to enhance FM coupling, one should increase the hole carrier density and increase the p–d exchange splitting [25]. However, large p–d coupling also leads to large localization of the hole state, thus, a balance between α and Δ_{pd} is needed; (c) for systems where Mn substitution on the cation site does not introduce holes (e.g. CdMnTe), the system is always more stable in the AFM phase. (d) For systems where Mn substitution on the cation site introduces holes (e.g. GaMnAs, where each Mn on Ga site introduces one hole), because the p–d coupling is larger than the d–d coupling, the system in general will have a FM ground state if enough holes are present in the system. However, when holes are compensated by donor defects, the system can revert to the AFM ground state.

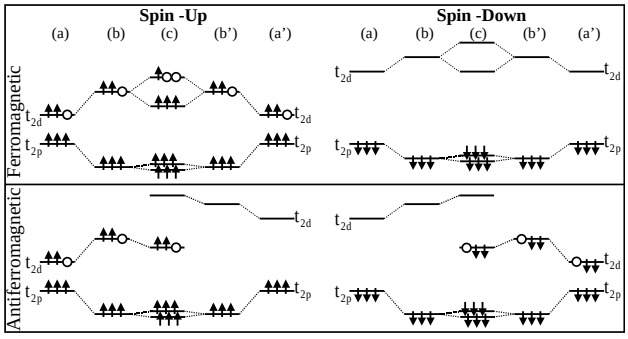

Fig. 3. Schematic model showing the position of the p and d levels and level repulsion between them in FM and AFM configurations. In this case, the Mn d levels are above the VBM. Note that in (b), (b′), and (c), the states have mixed pd characters.

In the second scenario we discuss the case when the Mn d state is above the VBM of the host. This is the case for Mn in ZnO or in GaN. A schematic plot is shown in Fig. 3. The analysis is similar to that in the first scenario. In the FM configuration and spin-up channel, the system not only gains energy through the p–d coupling by $-2m_h\Delta^1_{pd}$, but also through the d–d coupling [24] by $-m_h\Delta^1_{dd}$, which put holes at a high energy level and electrons at a low energy level. Here, $m_h\leq 3$ is the number of holes at the two t_{2d} level, and for simplicity, we still use Δ^1_{pd} to describe the coupling between the VBM and the majority t_{2d} state. The energy gain in the spin-down channel is $-12\Delta^2_{pd}$, thus the total energy gain for the FM configuration is $-m_h\Delta^1_{dd}-2m_h\Delta^1_{pd}-12\Delta^2_{pd}$. On the other hand, the net energy gain for the AFM configuration is $-(6-m_h)\Delta^{1,2}_{dd}-2m_h\Delta^1_{pd}-12\Delta^2_{pd}$, thus the energy difference between the FM and AFM phase is

$$\Delta E_{FM-AFM} = -m_h\Delta^1_{dd}+(6-m_h)\Delta^{1,2}_{dd}, \quad (2)$$

or

$$\Delta E_{FM-AFM} = -(6-m_h)\Delta^1_{dd}+(6-m_h)\Delta^{1,2}_{dd}, \quad (3)$$

if $m_h>3$. These results indicate that when the system has holes at the t_{2d}-derived level instead of the VBM, (a) the stabilization of the FM or AFM phase is not directly related to the p–d exchange splitting, but is determined by the d–d coupling [24] terms Δ^1_{dd} (often denoted as double exchange) and $\Delta^{1,2}_{dd}$. (b) When the number of holes m_h decreases, the AFM interaction increases. When $m_h=0$ (e.g. ZnMnO), the system is always more stable in the AFM phase. (c) The FM interaction is the largest when the t_{2d} levels are half filled. Therefore, by adjusting the number of holes (e.g. through n-type or p-type doping) one can enhance the magnetism. (d) Whether the system has an FM or AFM ground state depends not only on hole carrier density, but also on the relative strength of FM stabilization energy Δ^1_{dd}, and the AFM stabilization energy $\Delta^{1,2}_{dd}$. $\Delta^{1,2}_{dd}$ increases when the exchange splitting ε_{dd} decreases. This can be achieved if the charge is transferred from the majority to minority spin state (e.g. from majority t_{2d} to minority e_d state), thus reducing the magnetic moment and exchange splitting. The majority t_{2d} state can be pushed upward through increased p–d coupling, which can be realized by increasing Mn concentration or applying pressure.

3. Numerical test

To test our models, we performed first-principles total-energy calculations for CdMnTe, GaMnAs, ZnMnO, and GaMnN. The calculations were performed using an ab initio plane wave basis code [26], based on the local spin density functional theory and using ultrasoft pseudopotentials [27]. For the exchange and correlation potential, we used the generalized gradient approximation (GGA) of Perdew and Wang [28]. The Brillouin zone integration is performed using the Monkhost-Pack special **k** points scheme [29] of $4\times4\times4$ for the energy differences and $6\times6\times6$ for the density of states (DOS), in a 64 atom supercell with two Mn atoms as first fcc neighbors. Interactions of further neighbors were considered elsewhere [20]. We considered the zinc-blende alloy and assumed that the same results also hold for the alloy in a wurtzite structure.

Fig. 4 shows the total and Mn d projected density of states for CdMnTe and GaMnAs in the FM and AFM configurations. We see that these two systems correspond to scenario (i) where the VBM is between the majority and minority Mn d states. For CdMnTe, the substitution of Mn for Cd does not introduce holes (Fig. 4(a) and (b)), therefore, according to our model (Eq. (1)), the system should be AFM. For GaMnAs, holes are present in the VBM-derived states (Fig. 4(c) and (d)), therefore, our model predicts that it should be FM. Indeed, our directly calculated total energy differences between FM and AFM configurations for these two systems (Table 1) agree with those

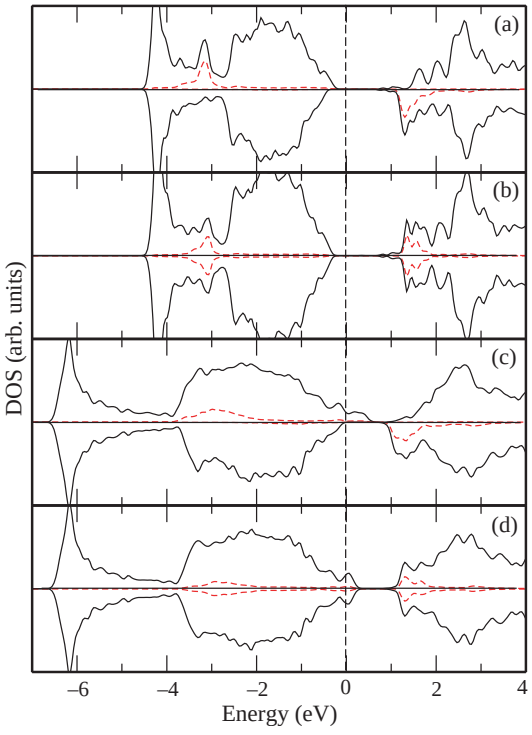

Fig. 4. (Color online) Total (solid) and Mn d projected (dashed) density of states for CdMnTe and GaMnAs: (a) ferromagnetic CdMnTe; (b) antiferromagnetic CdMnTe; (c) ferromagnetic GaMnAs; and (d) antiferromagnetic GaMnAs. The Fermi energy is at zero energy.

Table 1
Energy difference between FM and AFM configurations for Mn-doped semiconductors ($x=6.25\%$)

	$\Delta E_{\mathrm{FM-AFM}}$ (meV)	Ground state
$Cd_{1-x}Mn_xTe$	35	AFM
$Ga_{1-x}Mn_xAs$	−212	FM
$Zn_{1-x}Mn_xO$	110	AFM
$Ga_{1-x}Mn_xN$	−225	FM

expected from our model. Fig. 5 shows the total and Mn d projected density of states for ZnMnO and GaMnN in the FM and AFM configurations. We see that these two systems correspond to scenario (ii) where the VBM is below the Mn d states. For ZnMnO, no holes are present when Zn is replaced by Mn (Fig. 5(a) and (b)), therefore, according to our model (Eq. (2)), the system should be AFM. For GaMnN with small Mn concentration (6.25%), holes are created at the Mn 3d-derived level, and the Mn has a high-spin configuration (Fig. 5(c) and (d)), thus our model predicts that it should have an FM ground state. Again, our direct calculations shown in Table 1 agree with what is expected from our model.

The parameters from Eqs. (1) and (2) can, in principle, be estimated by changing the number of holes in the system [30]. We also want to point out that the results show in Table 1 are obtained from GGA, which somewhat underestimate the exchange splitting between the occupied and unoccupied d states. When the d–d exchange splitting is increased, e.g. by using LDA + U [31], the FM can be either suppressed such as in GaMnAs, or enhanced such as in GaMnN. This is because GaMnAs belong to scenario (i). From Eq. (1) and Fig. 1, we can see that when d–d exchange splitting increases, both Δ_{pd} and $\Delta_{\mathrm{dd}}^{1,2}$ decreases. Because the pd term dominates in GaMnAs, such a reduction will reduce FM. On the other hand, GaMnN belong to scenario (ii). From Eq. (2) and Fig. 1, we see that the direct FM Δ_{dd}^{1} coupling is not affected by the increase d–d exchange splitting, but the AFM superexchange $\Delta_{\mathrm{dd}}^{1,2}$ term decreases. Thus, FM in GaMnN is enhanced when d–d exchange splitting increases. These observations are consistent with previous LDA + U calculations [31].

4. Magnetic order of $Ga_{1-x}Mn_xN$

We have performed further tests on $Ga_{1-x}Mn_xN$ to understand its intriguing behavior of different magnetic ordering as a function of Mn concentration x and carrier density. The calculations for this case were done using supercells with 32 atoms. The disorder effects of the alloy is taken into account explicitly through the special quasirandom structure approach [32]. For AFM calculations involving more than two Mn atoms, the sign of the magnetic moments on each Mn site is initially distributed randomly. For the cases where the AFM configuration was higher in energy than the FM phase, several other AFM configurations are tested to make sure that the FM phase indeed has the lowest total energy.

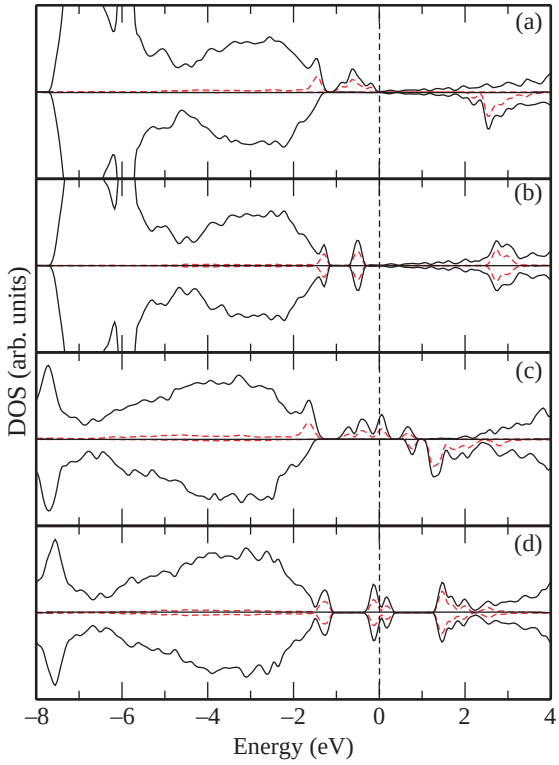

Fig. 5. (Color online) Total (solid) and Mn d projected (dashed) density of states for ZnMnO and GaMnN: (a) ferromagnetic ZnMnO; (b) antiferromagnetic ZnMnO; (c) ferromagnetic GaMnN; and (d) antiferromagnetic GaMnN. The Fermi energy is at zero energy.

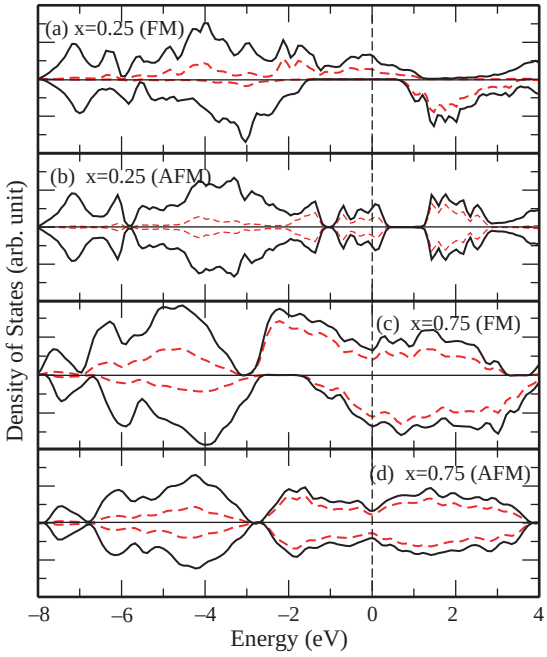

Fig. 6. (Color online) Total (solid) and Mn_d projected (dashed) density of states for $Ga_{1-x}Mn_xN$ with different concentrations and magnetic configurations. The Fermi energy is at zero energy.

We find that unlike $Ga_{1-x}Mn_xAs$, where the ground state is always FM, in $Ga_{1-x}Mn_xN$, the magnetic ground state changes with Mn concentration x. At low Mn concentrations, our calculations show that the FM phase of the Mn atoms is more stable, as discussed before and in agreement with other previous theoretical calculations [33]. However, at high Mn concentrations, the lowest energy state becomes AFM. To explain this interesting behavior, we can use our model described in Fig. 3 and Eq. (2): at low Mn concentration, because the p–d repulsion is weak, the exchange splitting of the Mn d orbitals is larger than their crystal field splitting (Fig. 3), so the system has a high-spin configuration and the FM interaction Δ^1_{dd} is larger than the AFM interaction $\Delta^{1,2}_{dd}$. When the Mn concentration increases, the crystal field splitting increases due to the larger p–d repulsion. The majority t_{2d} levels are pushed higher in energy, and the dispersion of the Mn d band also increases. When part of the majority spin t_{2d} levels becomes higher than the minority spin e_d state, charge transfer will occur between these two states, which will lead to a low-spin configuration with reduced spin exchange splitting. Because reduced spin exchange splitting will enhance the AFM coupling between the Mn d majority state and the minority state ($\Delta^{1,2}_{dd}$), the system will become increasingly stable in the AFM phase when the Mn concentration increases.

In Fig. 6 we plotted the total and the projected DOS of $Ga_{1-x}Mn_xN$ with $x=0.25$ and $x=0.75$, which has FM and AFM ground states, respectively. From the calculated projected density of states, we find that at $x=0.25$, in the FM case, the holes are created in the spin-up channel, whereas in the AFM phase, the holes are created in both spin channels. The calculated magnetic moment is $3.59\mu_B$ for the FM phase and $3.32\mu_B$ in the AFM phase. The reason that the FM phase has a larger magnetic moment is because the AFM coupling shown in Fig. 3 mixes filled and empty d states [34], thus reducing the magnetic moment in the AFM phase. At $x=0.75$, the increase of the Mn concentration also increases the p–d repulsion, leading to a large overlap between the majority spin t_{2d} levels and the minority spin e_d levels. Due to the charge transfer between the majority spin and minority spin states, the minority e_d state is partially occupied and the magnetic moment is reduced. In the FM and AFM phases, the calculated magnetic moments are 1.96 and $2.40\mu_B$, respectively. In this case, the FM phase has a smaller moment than the AFM phase, opposite to that at low Mn concentration. This is because at higher concentration, the charge transfer from the spin-up t_{2d} level to the spin-down e_d level is larger in the FM phase than in the AFM phase. We see that the calculated results are consistent with our model.

Our discussion above shows that the change from FM to AFM in GaMnN when Mn concentration increases is due to the increased crystal field splitting and band broadening, which leads to a reduced Mn d–d spin exchange splitting. We notice that the same effect can also be simulated by applying pressure (or reducing the lattice constant). This is because under pressure, the increased p–d coupling increases the crystal field splitting. To test this, we repeated the calculation at $x=0.25$, but at a lattice constant that is 10% smaller than the equilibrium lattice constant. We find that under this

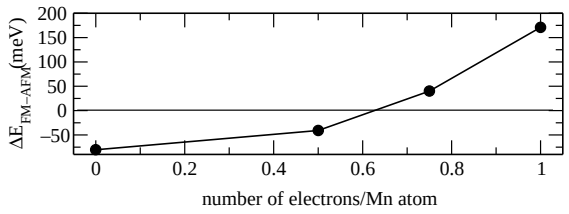

Fig. 7. Energy difference between ferromagnetic and antiferromagnetic configurations as a function of the number of electrons added per Mn atom in $Ga_{0.75}Mn_{0.25}N$.

compression, the system indeed becomes more stable in the AFM phase, whereas at its equilibrium lattice constant, it is more stable in the FM phase. The magnetic moment in this case is also reduced, being $2.48\mu_B$ for the AFM phase and $2.41\mu_B$ for the FM phase, similar to the case of high concentrations. A similar effect was previously observed in the surface of GaN, where the distance between Mn atoms is smaller [11].

Our model also suggests that at low Mn concentration, $Ga_{1-x}Mn_xN$ is more stable in the FM phase when holes are in the Mn d bands, whereas the AFM phase will be more stable when the holes are filled. To test this, we have calculated the energy difference between the FM and AFM phases ΔE_{FM-AFM} for $Ga_{1-x}Mn_xN$ as a function of the number of electrons added per Mn atom at $x=0.25$. The results are plotted in Fig. 7. We find that, indeed, the system becomes more stable in the AFM phase when the added electron reaches 0.62 per Mn atom. This is in agreement with our prediction from Eq. (2) and should also be true for the case of GaMnAs. Similar results for the stabilization of the AFM phase through hole compensation have been reported before [35]. We also notice that the lattice constant increases when Mn is negatively charged because of the larger Coulombic repulsion between anions and the negatively charged Mn atom. This suggests that the AFM phase is possible in GaMnN if the Mn atoms are compensated by donors such as Mn interstitials, N vacancies, or N_{Ga} antisite defects.

5. Conclusions

In summary, we have proposed a model that can successfully explain the stabilization of the ferromagnetic or antiferromagnetic ordering in Mn-doped II–VI and III–V semiconductors. This simple model is based on the p–d and d–d level repulsions between the Mn ions and host states and can be directly related to band parameters. Therefore, it should be very useful in understanding and engineering diluted magnetic semiconductors with desired properties. A similar model could also be developed to study other transition metals in semiconductors, as long as the position of the d levels and the number of holes induced by it were known.

Acknowledgements

The work at NREL is funded by the US Department of Energy, Office of Science, Basic Energy Sciences, under Contract No. DE-AC36-99GO10337 to NREL. XGG is supported by the Nature Science Fundation of China, Chinese Academy of Science, and National Science Foundation of China. AF and AJRS thank the support from CNPq and FAPESP.

References

[1] J.K. Furdyna, J. Kossut (Eds.), Diluted magnetic Semiconductors, Academic Press, Boston, 1988.
[2] H. Ohno, Science 281 (1998) 951.
[3] T. Dietl, et al., Science 287 (2000) 1019.
[4] D.D. Awschalom, et al., Nature 408 (2000) 923.
[5] S.A. Wolf, et al., Science 294 (2001) 1488.
[6] M.E. Overberg, et al., Phys. Lett. 79 (2001) 1312.
[7] M.L. Reed, et al., Appl. Phys. Lett. 79 (2001) 3473.
[8] N. Theodoropoulou, et al., Appl. Phys. Lett. 78 (2001) 3475.
[9] Y. Shon, et al., Appl. Phys. Lett. 79 (2002) 1845.
[10] M. Zajac, et al., Appl. Phys. Lett. 79 (2001) 2432.
[11] Q. Wang, et al., Phys. Rev. Lett. 93 (2004) 155501.
[12] S. Dhar, et al., Appl. Phys. Lett. 82 (2003) 2077.
[13] L. Kronik, et al., Phys. Rev. B 66 (2002) 041203(R).
[14] S.J. Pearton, et al., J. Phys.: Condens. Matter 16 (2004) R209.
[15] T. Dietl, et al., MRS Bull. (2003) 714.
[16] V.I. Litvinov, et al., Phys. Rev. Lett. 86 (2001) 5593.
[17] K. Sato, et al., Eur. Phys. Lett. 61 (2003) 403.
[18] M. van Schilfgaarde, et al., Phys. Rev. B 63 (2001) 233205.
[19] In a first-order approximation, including spin–orbit coupling will not change the magnetic stability qualitatively. See Ref. [20].
[20] A.J.R. da Silva, et al., J. Phys.: Condens. Matter 16 (2004) 8243.
[21] S.-H. Wei, et al., Phys. Rev. Lett. 56 (1986) 2391.
[22] J. Wu, et al., Semicond. Sci. Technol. 17 (2002) 860.
[23] K.S. Burch, et al., Phys. Rev. B 70 (2004) 205208.
[24] Although the coupling is denoted as d–d for simplification, due to the strong p–d hybridization between the t_{2d} and t_{2p} states, the states in (b), (b′), and (c) in Figs. 2 and 3 have mixed pd characters. Because of this hybridization, the so-called d–d coupling is not exactly a short-range interaction.
[25] M. Csontos, et al., Nat. Mater 4 (2005) 447.
[26] (a) G. Kresse, et al., Phys. Rev. B 47 (1993) RC558;
(b) G. Kresse, et al., Phys. Rev. B 54 (1996) 11169.
[27] D. Vanderbilt, Phys. Rev. B 41 (1990) 7892.
[28] J.P. Perdew, et al., Phys. Rev. B 45 (1992) 13244.
[29] H.J. Monkhorst, et al., Phys. Rev. B 13 (1976) 5188.
[30] G.M. Dalpian, et al., In preparation.
[31] (a) L.M. Sandratskii, et al., Phys. Rev. B 69 (2004) 195203;
(b) A.B. Shick, et al., Phys. Rev. B 69 (2004) 125207;
(c) J.H. Park, et al., Physica B 281–282 (2000) 703.
[32] S.-H. Wei, et al., Phys. Rev. B 42 (1990) 9622.
[33] B. Sanyal, et al., Phys. Rev. B 68 (2003) 205210.
[34] S.-H. Wei, et al., Phys. Rev. B 71 (2005) 144409.
[35] K. Sato, et al., Semicond. Sci. Technol. 17 (2002) 367.